Reaction Chemistry & Engineering

ROYAL SOCIETY OF CHEMISTRY

COMMUNICATION

View Article Online
View Journal | View Issue

Cite this: *React. Chem. Eng.*, 2025, **10**, 511

Received 12th July 2024,
Accepted 6th December 2024

DOI: 10.1039/d4re00339j

rsc.li/reaction-engineering

Self-optimising continuous-flow hydrothermal reactor for nanoparticle synthesis†

Cameron Jackson,[a] Karen Robertson,[a] Vitaliy Sechenyh,[a] Thomas W. Chamberlain,[b] Richard A. Bourne[c] and Edward Lester *[a]

An autonomous continuous-flow, hydrothermal synthesis reactor, capable of self-optimising nanoparticle size using an in-line characterisation technique and machine learning is presented. The developed system is used for synthesis of hematite (α-Fe_2O_3) nanoparticles across three process variables, optimising for a target particle size. Optimisation is achieved in under 7 h with only 500 ml of 0.1 M $Fe(NO_3)_3{\cdot}9H_2O$ aqueous stock solution used, and without human intervention.

Nanomaterials have numerous applications including catalysis,[1–3] optics,[4] drug delivery[5–7] and energy storage,[8,9] whilst low-cost iron oxide nanomaterials have potential utilization in pigments,[10] wastewater treatments[11] and photovoltaic devices.[12] Hematite (α-Fe_2O_3) has previously been proven to be highly controllable in terms of size and shape of nanoparticles using hydrothermal synthesis.[13–15]

Hydrothermal synthesis has traditionally been a batch process, which has served to limit production at large scale.[16] Continuous-flow synthesis demonstrates many distinct advantages over traditional batch methods, such as enhanced control of heat and mass transfer, reduced batch variability and the ability to quickly modify and screen synthesis conditions.[17,18] Flow systems can be further enhanced with the incorporation of online process analytical technologies (PATs)[19] to provide real-time information on particle size, morphology or composition; these parameters are key attributes in the synthesis of nanoparticles and can significantly alter the physicochemical properties of the final product.[20]

First reported in 1992 by Adschiri *et al.*,[21] continuous-flow hydrothermal synthesis (CFHS) of nanomaterials has been demonstrated as a green and scalable alternative to traditional nanoparticle synthesis techniques.[22] Hydrothermal synthesis involves the heating of precursor solutions above their standard boiling point in a pressurised reactor. As water is heated to near, or above, its critical point (647.15 K and 22.4 MPa), it exhibits vastly different properties, such as reduced density and polarity,[23] which can be actively exploited for the controlled synthesis of nanoparticles.[24–26] The increased dissociation of water at near-critical conditions leads to high concentrations of H^+ and OH^- ions, which can then be used for the immediate hydrolysis and dehydration of metal salt precursors, resulting in the precipitation of metal oxide nanoparticles.[27] Historically, ferrihydrite was the first stable product synthesised using CFHS through hydrolysis of iron precursors.[28,29] The transition of ferrihydrite to more stable forms such as goethite, akaganeite or hematite was found to be dependent on temperature, pH and synthesis time.[30]

Automation of continuous flow synthesis can often reduce the time and cost required to optimise materials.[31] One of the earliest examples of self-optimisation in a continuous flow reactor is the synthesis of CdSe quantum dot nanoparticles, using inline spectroscopy.[32] Recent advances in both process equipment and supervised machine learning (SML) methods provide exciting potential in creation of "autonomous reactors".[33] Such cyber-physical reactors have demonstrated the ability to finely tune particle size in continuous flow systems by integrating more complex reactor designs, reaction chemistries or machine learning and optimisation strategies into nanoparticle flow synthesis.[34–38]

Here we present self-optimisation of hematite particles targeting a maximum particle size (with an acceptably low size distribution) in a benchtop autonomous millifluidic supercritical hydrothermal reactor, combined with inline dynamic light scattering (DLS). The system is integrated with supervised machine learning methods (SNOBFIT and a

[a] *Advanced Materials Research Group, Faculty of Engineering, University of Nottingham, Nottingham NG7 2RD, UK. E-mail: Eczehl@exmail.nottingham.ac.uk*
[b] *Institute of Process Research and Development, School of Chemistry, School of Chemical and Process Engineering, University of Leeds, Leeds, UK*
[c] *School of Chemical and Process Engineering, University of Leeds, Leeds LS2 9JT, UK*

† Electronic supplementary information (ESI) available. See DOI: https://doi.org/10.1039/d4re00339j

custom Bayesian-optimised Gaussian process) to enable autonomous exploration and optimisation of process conditions; the process is iterative and continues to generate and execute experiments until either converging upon the optimum conditions or reaching the maximum number of experiments. Each process took <7 hours to complete and used only 500 ml of $Fe(NO_3)_3{\cdot}9H_2O$ solution for the pre-set 30 samples. The optimisers were targeted for maximum particle size using inline DLS analysis, validated through offline PXRD and TEM characterisation. The maximum particle size obtained was 27 nm for a residence time of 1.6 s.

The CFHS used here (Fig. 1) has been published previously.[25,39] In this study, aqueous $Fe(NO_3)_3$ (upflow) is delivered at room temperature to the counter-current mixing point of the nozzle reactor[40,41] with pre-heated deionised water (downflow), thus precipitating Fe_2O_3 nanoparticles. 0.1 M stock solution of $Fe(NO_3)_3$ is diluted in flow *via* a dilution pump of deionised water to achieve a wide concentration ratio of upflow : downflow whilst enabling independent exploration of total flowrate. The pressure of the reactor is maintained at 24 MPa throughout. Dilute nitric acid was used for the flush stage to remove any particle fouling from within the reactor between each experiment. Inline particle analysis was achieved through employing a Zetasizer Nano ZS (Malvern Panalytical Ltd) with a custom sampling system for parallel injection into the flowcell (ZEN0023, Malvern), mitigating limitation of the maximum process flowrate. Validation of inline results was carried out by powder X-ray diffraction (PXRD, Bruker D8-Advance Da Vinci Diffractometer with Cu Kα radiation, λ = 1.5418 Å) and transmission electron microscopy (TEM, JEOL 2100F HRTEM equipped with a field emission gun (FEG) and operating at 100 kV).

An initial DoE (Table 1, ESI†) was used to establish the range of closed-loop self-optimisation. The custom SML algorithm employed uses a combination of Bayesian optimisation and Gaussian Process Regression (GPR) models (Fig. S4, ESI†). The code of the self-optimisation algorithm is created using Statistics and Machine Learning Toolbox and MATLAB 9.10.0.1684407 (2021a). We also compare the self-optimisation with a common global optimiser, SNOBFIT (Stable Noisy Optimisation by Branch and Fit).[42,43] For each optimisation method, a 3-level full factorial design was employed with optimisation for maximum particle size within 30 experiments. Samples with a polydispersity index (PDI) >0.5 were considered invalid. To encourage exploration of the design space, experiments were generated in batches of six; the optimisation algorithm then schedules the experiment closest to the target response, followed by randomly selected sets of variables across the design space.[44,45]

We used a Bayesian optimiser which explores areas of uncertainty against available data points.[46–48] This approach can remain relatively robust, in the presence of experimental

Table 1 Synthesis conditions and particle size (by DLS, PXRD and TEM) obtained by online dynamic light scattering analysis. Flow ratio is calculated between upflow and total flow rate

	Downflow temperature [°C]	Flowrate [ml min^{-1}]	Flow ratio	DLS [nm]	PXRD [nm]	TEM [nm]
A	360	30.0	0.365	45.4	10.0	5.4 ± 3.0
B	367	28.1	0.356	54.1	10.3	7.1 ± 4.1
C	370	30.0	0.330	67.0	15.0	9.1 ± 2.7
D	380	27.4	0.369	76.2	18.2	10.7 ± 3.2
E	380	26.0	0.330	84.1	22.6	27.1 ± 8.2
F	380	25.0	0.330	91.7	23.7	27.0 ± 7.8

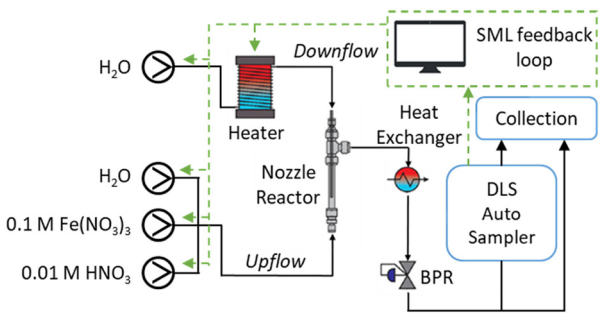

Fig. 1 Schematic of the CFHS reactor highlighting supervised machine learning (SML) loop. BPR: back-pressure regulator.

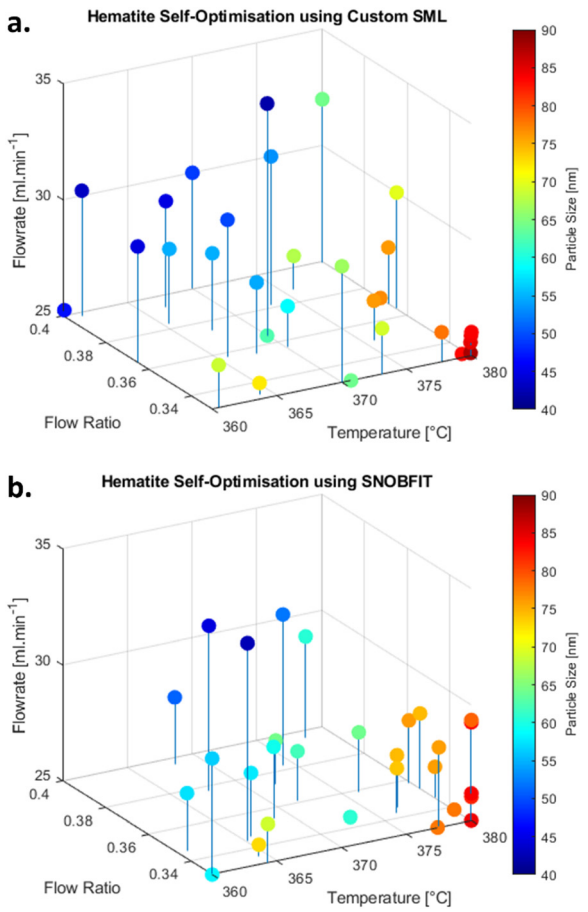

Fig. 2 4D scatter plot of experiments showing particle size from a. the custom SML study and b. the SNOBFIT study.

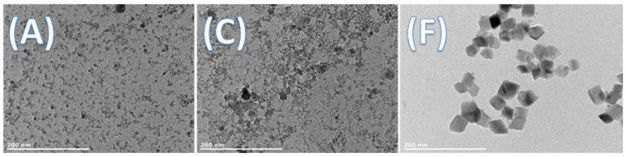

Fig. 3 TEM images of hematite samples A, C and F (left to right). Scale bar at 200 nm.

noise, making it an excellent way to optimise processes in the fewest possible experiments. This approach is discussed in more detail by Clayton and co-workers.[49]

The outcomes of self-optimised experiments are presented in Fig. 2a and b. Both optimisation methods demonstrated similar behaviour of the response with respect to changes in process variables, showing an increased particle size at elevated temperature, reduced flow ratio and higher residence times. This result agrees well with literature where hematite nanoparticles were produced using batch process with the nucleation, phase transition and growth of hematite particles during synthesis.[50] PXRD analysis confirms the presence of hematite in all samples selected for offline analysis but shows contamination from $NaNO_3$ in samples E and F (Fig. S16, ESI†). This is presumed to be contamination due to NO_3^{2-} ions and Na^+ ions present in the DI water.

TEM images (Fig. 3) for all studied samples demonstrated various stages in the generation and growth of hematite nanoparticles (section 5, ESI†). Samples A and B (lowest temperature and fastest flowrate) primarily revealed spherical-cubic particles in the range 5–12 nm. This corresponds to the peak broadening shown in the PXRD patterns for these samples. Samples E and F (highest temperature and lowest flowrate) have distinct cubic α-Fe_2O_3 particles, suggesting the particles have undergone Ostwald ripening, according to the LaMer model of nanomaterial synthesis.[51] Application of the Scherrer equation to the PXRD patterns yields comparable particle sizes but the inline DLS measurements are shown to significantly overestimate particle size (Table 1 & sections 1, 2 and 4, ESI†), although the trend is comparable. This suggests that inline DLS may not be feasible for obtaining absolute values but is still appropriate for trend targeting, which is the main aim of this study.

This paper outlines the first use of a DLS technique for a self-optimised, continuous-flow hydrothermal synthesis reactor. Automated analysis and reactor control are combined with self-optimisation algorithms to achieve maximum particle size of hematite nanoparticles in under 7 h per optimisation experiment with only 500 ml reagent use. The use of the applied algorithm approach (based on ESI† Tables S2 and S3) shows that the maximum particle size was identified after only 9 of the 30 experiments in the factorial design. TEM images show the formation of small particles prior to aggregation and subsequent growth of hematite particles. DLS, XRD and TEM are all used to provide particle size analysis, with DLS hydrodynamic diameters showing significantly larger measurements. Calibration of DLS method using TEM data as a reference could enable optimisation and tuning of the particle size in real time. The system presented is designed to be suitable to a range of nanomaterials already demonstrated for CFHS and can be used to efficiently determine the effects of different parameters such as temperature, precursor concentration or reaction time on the particle size and distribution.

Data availability

The data supporting this article have been included as part of the ESI.†

Author contributions

Cameron Jackson: Conceptualization, methodology, formal analysis, investigation, validation, visualization, writing, editing. Vitaliy Sechenyh: Formal analysis, validation, visualization, writing, editing. Karen Robertson: Conceptualization, supervision, formal analysis, writing, editing. Thomas Chamberlain: Conceptualization, project administration, funding acquisition, editing. Richard Bourne: Conceptualization, project administration, funding acquisition, editing. Edward Lester: Conceptualization, methodology, formal analysis, supervision, project administration, funding acquisition, editing.

Conflicts of interest

The authors declare that there are no conflicts of interest.

Acknowledgements

The authors acknowledge the support of the project by the EPSRC [Grant number EP/R032807/1] and Promethean Particles Ltd. TEM images courtesy of Michael Fay (Nanoscale and Microscale Research Centre, Nottingham, United Kingdom).

Notes and references

1 S. Ko and J. Jang, *Angew. Chem., Int. Ed.*, 2006, **45**, 7564.
2 H. Yoon, S. Ko and J. Jang, *Chem. Commun.*, 2007, 1468.
3 B. Choi, H. Yoon, I.-S. Park, J. Jang and Y.-E. Sung, *Carbon*, 2007, **45**, 2496.
4 K. C. Park, H. J. Choi, C. H. Chang, R. E. Cohen, G. H. McKinley and G. Barbastathis, *ACS Nano*, 2012, **6**(5), 3789–3799.
5 P. Yang, Z. Quan, L. Lu, S. Huang and J. Lin, *Biomaterials*, 2007, **29**, 692.
6 S. Guo, D. Li, L. Zhang, J. Li and E. Wang, *Biomaterials*, 2009, **30**, 1881.
7 W.-K. Oh, H. Yoon and J. Jang, *Biomaterials*, 2010, **31**, 1342.
8 S. H. Moon, W. J. Jin, T. R. Kim, H. S. Hahm, B. Cho and M.-S. Kim, *J. Ind. Eng. Chem.*, 2005, **11**, 594.
9 M. Choi and J. Jang, *J. Colloid Interface Sci.*, 2008, **325**, 287.

10 EFSA, Scientific Opinion on the re-evaluation of iron oxides and hydroxides (E 172) as food additives, *EFSA J.*, 2015, **13**, 4317, EFSA Panel on Food Additives.
11 P. Xu, G. M. Zeng, D. L. Huang, C. L. Feng, S. Hu, M. H. Zhao, C. Lai, Z. Wei, C. Huang, G. X. Xie and Z. F. Liu, *Sci. Total Environ.*, 2012, **424**, 1–10.
12 F. Cai, S. Zhanga and Z. Yuan, *RSC Adv.*, 2015, **53**, 42869–42874.
13 K. Byrappa and T. Adschiri, *Prog. Cryst. Growth Charact.*, 2007, **53**, 117–166.
14 T. Almeida, M. Fay, Y. Zhu and P. Brown, *Nanoscale*, 2010, **2**, 2390–2399.
15 M. Zhu, Y. Wang, D. Meng, X. Qin and G. Diao, *J. Phys. Chem. C*, 2012, 16276–16285.
16 O. Dlugosz and M. Banach, *React. Chem. Eng.*, 2020, **5**, 1619–1641.
17 H. A. Elazab, S. Moussa, K. W. Brinkley, B. F. Gupton and M. S. El-Shall, *Green Process. Synth.*, 2017, **6**, 413–424.
18 A. M. Nightingalea and J. C. Mello, *J. Mater. Chem.*, 2010, **20**, 8454–8463.
19 L. X. Yu, R. A. Lionberger, A. S. Raw, R. D'Costa, H. Wu and A. S. Hussain, *Applications of process analytical technology to crystallization processes*, FDA CDER, Rockville, MD, 2003.
20 H. W. Kang, J. Leem, S. Y. Yoona and H. J. Sung, *Nanoscale*, 2013, **6**, 2840–2846.
21 T. Adschiri, K. Kanazawa and K. Arai, *J. Am. Ceram. Soc.*, 1992, **75**, 1019–1022.
22 T. Adschiri, Y. W. Lee, M. Goto and S. Takami, *Green Chem.*, 2011, **13**, 1380–1390.
23 H. Weingärtner and E. U. Franck, *Angew. Chem., Int. Ed.*, 2005, **44**, 2672–2692.
24 P. W. Dunne, A. S. Munn, C. L. Starkey, T. A. Huddle and E. H. Lester, *Philos. Trans. R. Soc.*, 2015, **373**, 0015.
25 A. S. Munn, P. W. Dunne, S. V. Y. Tang and E. H. Lester, *Chem. Commun.*, 2015, **51**, 12811–12814.
26 E. Lester, P. Blood, J. Denyer, D. Giddings, B. Azzopardia and M. Poliakoff, *J. Supercrit. Fluids*, 2006, **37**, 209–214.
27 M. Lin, H. R. Tan, J. P. Y. Tan and S. Bai, *J. Phys. Chem. C*, 2013, **117**, 11242–11250.
28 J. S. Weatherill, K. Morris, P. Bots, T. M. Stawski, A. Janssen, L. Abrahamsen, R. Blackham and S. Shaw, *Environ. Sci. Technol.*, 2016, **50**, 9333–9342.
29 R. M. Cornell and U. Schwertmann, *The Iron Oxides. Structure, Properties, Reactions, Occurences and Uses*, Wiley-VCH, 2nd edn, 2003.
30 Y. Cudennec and A. Lecerf, *J. Solid State Chem.*, 2006, **179**, 716–722.
31 B. K. H. Yen, A. Gunther, M. A. Schmidt, K. F. Jensen and M. G. Bawendi, *Am. Ethnol.*, 2005, **44**, 5447–5451.
32 S. Krishnadasan, R. J. C. Brown, A. J. de Mello and J. C. de Mello, *Lab Chip*, 2007, **11**, 1434–1441.
33 C. Mateos, M. J. Nieves-Remacha and J. A. Rincón, *React. Chem. Eng.*, 2019, **4**, 1536–1544.
34 L. Wang, L. R. Karadaghi, R. L. Brutchey and N. Malmstadt, *Chem. Commun.*, 2020, **56**, 3745–3748.
35 K. Abdel-Latif, R. W. Epps, F. Bateni, S. Han, K. G. Reyes and M. Abolhasani, *Adv. Intell. Syst.*, 2021, **3**, 2000245.
36 L. Bezinge, R. M. Maceiczyk, I. Lignos, M. V. Kovalenko and A. J. deMello, *ACS Appl. Mater. Interfaces*, 2018, **10**, 18869–18878.
37 R. W. Epps, M. S. Bowen, A. A. Volk, K. Abdel-Latif, S. Han, K. G. Reyes, A. Amassian and M. Abolhasani, *Adv. Mater.*, 2020, **32**, 2001626.
38 A. A. Volk, R. W. Epps and M. Abolhasani, *Adv. Mater.*, 2021, **33**, 2004495.
39 I. Clark, R. L. Gomes, C. Crawshaw, L. Neve, R. Lodge, M. Fay, C. Winkler, M. Hulle and E. Lester, *React. Chem. Eng.*, 2019, **4**, 663–666.
40 C. Jackson, A self-optimising continuous-flow hydrothermal reactor for nanomaterial synthesis, *PhD thesis*, University of Nottingham, United Kingdom, 2021.
41 E. Lester, "Counter Current Mixing Reactor", *UK Pat.* WO2005077505, 2005.
42 S. M. Moosavi, L. Talirz and B. Smit, *Synthesis Condition Finder*, 2019, DOI: **10.5281/zenodo.1312814**.
43 W. Huyer and A. Neumaier, *ACM Trans. Math. Softw.*, 2008, **35**, 1–25.
44 A. D. Clayton, J. A. Manson, C. J. Taylor, T. W. Chamberlain, B. A. Taylor, G. Clemens and R. A. Bourne, *React. Chem. Eng.*, 2019, **4**, 1545–1554.
45 N. Holmes, G. R. Akien, A. J. Blacker, R. L. Woodward, R. E. Meadows and R. A. Bourne, *React. Chem. Eng.*, 2016, **1**, 366–371.
46 M. Schweidtmann, A. D. Clayton, N. Holmes, E. Bradford, R. A. Bourne and A. A. Lapkin, *Chem. Eng. J.*, 2018, **352**, 277–282.
47 B. J. Shields, J. Stevens, J. Li, M. Parasram, F. Damani, J. I. M. Alvarado, J. M. Janey, R. P. Adams and A. G. Doyle, *Nature*, 2021, **590**, 89–96.
48 K. Y. Nandiwale, T. Hart, A. F. Zahrt, A. M. K. Nambiar, P. T. Mahesh, Y. Mo, M. J. Nieves-Remacha, M. D. Johnson, P. García-Losada, C. Mateos, J. A. Rincón and K. F. Jensen, *React. Chem. Eng.*, 2022, **7**, 1315–1327.
49 A. D. Clayton, E. O. Pyzer-Knapp, M. Purdie, M. Jones, A. Barthelme, J. Pavey, N. Kapur, T. W. Chamberlain, A. J. Blacker and R. A. Bourne, *Angew. Chem.*, 2023, **62**, 1591.
50 S. P. Schwaminger, R. Surya, S. Filser, A. Wimmer, F. Weigl, P. Fraga-García and S. Berensmeier, *Sci. Rep.*, 2017, **7**, 12609.
51 J. S. Weatherill, K. Morris, P. Bots, T. M. Stawski, A. Janssen, L. Abrahamsen, R. Blackham and S. Shaw, *Environ. Sci. Technol.*, 2016, **50**, 9333–9342.